RSC Advances

PAPER

View Article Online
View Journal | View Issue

Cite this: *RSC Adv.*, 2014, **4**, 63128

Size-dependent photoluminescence of zinc oxide quantum dots through organosilane functionalization†

Viorica Muşat,*[a] Aurel Tăbăcaru,[a] Bogdan Ştefan Vasile[b] and Vasile-Adrian Surdu[b]

Received 20th September 2014
Accepted 10th November 2014

DOI: 10.1039/c4ra10851e

www.rsc.org/advances

Organosilane grafting on the surface of ZnO nanoparticles is a possible means of fabricating hybrid nanomaterials with tuned optical and physico-chemical properties. We report here the synthesis, morpho-structural characterization and optical properties of hybrid ZnO quantum dots (QDs) grafted with variable amounts of the surfactant 3-(trimethoxysilyl)propylmethacrylate (MPS) (2, 5 and 10% molar ratios of Si/Zn). This organosilane surfactant was chosen to evaluate its ability to both prevent the agglomeration of the nanoparticles and to tune the optical properties of the resulting hybrid nanomaterials. The grafted ZnO QDs were prepared using a modified precipitation method and were characterized by X-ray diffraction, high-resolution transmission electron microscopy, Fourier transform infrared spectrometry and thermogravimetric analysis; their optical properties were studied by UV-visible spectrometry. Unmodified ZnO and MPS-grafted ZnO QDs showed optical transmittance between 85 and 90% and low reflectance in the visible domain, whereas a significant blue shift of the photoemission bands was observed from 578 nm in unmodified ZnO to 546 nm in ZnO grafted with 10% MPS. This shift is associated with the reduction in size of the ZnO QDs with increasing amounts of MPS. A decrease in the band gap energies from 3.494 eV for unmodified ZnO to 3.377 eV for ZnO–MPS 10% was detected and gives a new insight into the relationship between the reduction in nanoparticle size promoted by an organic surfactant with electron injection into the ZnO bands and the value of band gap energy.

1. Introduction

ZnO nanoparticles have been the subject of much research over a number of scientific disciplines and have many potential applications, *e.g.* in optics, electronics, optoelectronics (light-emitting diodes), UV lasers and photodetectors,[1] solar cells[2] and thin film transistors.[3] This metal oxide semiconductor, with a wide band gap (3.37 eV) and high exciton binding energy (60 meV) at room temperature, has also been used in many other applications, including gas sensing,[4] catalysis,[5] cell labelling[6] and as an antifouling,[7] photocatalytic and antibacterial[8] agent.

Many of these applications require the properties of the nanoparticle surfaces to be controlled. The optical and opto-electronic properties, in particular, are essentially dependent on the size of the nanoparticles. A crucial disadvantage in practical applications is the tendency of the nanoparticles to agglomerate and it is therefore important to be able to control the particle size and surface properties. Stabilization through the organic functionalization of the surface of ZnO nanoparticles is a useful strategy for controlling and, eventually, suppressing their agglomeration, growth and surface defects.[9,10] It is possible to attain a significant reduction in the particle size to the level of quantum dots (QDs) by applying strategic surface grafting, thus allowing the optical, photoluminescent and physico-chemical properties to be tuned. Several reports have started to address this trend of surface modification with grafting of the ZnO surface with different organic species such as thiols,[10] polymers[11] and alkylamines.[12]

We report here a study of one promising organosilane: 3-(trimethoxysilyl)propylmethacrylate (MPS). The reactive alkoxy functional groups of MPS provide strong and stable chemical bonds with inorganic species after hydrolysis followed by condensation reactions. Despite this useful reactivity towards surface modification, only a few reports have described the synthesis of MPS-grafted ZnO nanoparticles together with detailed NMR spectroscopic characterization of the structural organization of the hydrolysed MPS molecules on the ZnO surface.[13,14] The incorporation of a very small number of organic surfactant-grafted ZnO nanoparticles into transparent

[a]*Center of Nanostructures and Functional Materials – CNMF, Faculty of Engineering, Dunărea de Jos University of Galati, 111 Domneasca Street, 800201, Galați, Romania. E-mail: viorica.musat@ugal.ro; Tel: +40-757070613*

[b]*University Politehnica of Bucharest, Faculty of Applied Chemistry and Materials Science, Department of Science and Engineering of Oxide Materials and Nanomaterials, Polizu Street no. 1-7, 011061, Bucharest, Romania*

† Electronic supplementary information (ESI) available: Synthesis of ZnO nanoparticles, crystallografic data, electron diffraction patterns, infrared spectrum of free MPS, reaction schemes for MPS grafting of ZnO nanoparticles, and table containing their stoichiometric formulations. See DOI: 10.1039/c4ra10851e

nanocomposite films for the study of optical and photoluminescent properties has been reported previously.[15,16]

Recognizing the potential of MPS to establish stable covalent bonds by surface grafting on ZnO, with a direct influence on its structure, morphology and electronic features, we obtained and characterized a series of MPS-grafted ZnO QDs using different molar ratios of Zn/Si (2, 5 and 10%). A systematic study of the optical properties of this series (transmittance, reflectance and photoluminescence) was undertaken. The choice of this type of organosilane surfactant is part of our strategy to explore the tuning of optical properties taking into account the nature of the end-group bound to silicon. Silicon-based species are known to have very good cohesion and adhesion on hydrolysis when deposited as films or layers on rigid or flexible substrates to achieve hybrid light-emitting devices with high stability and transparency.[17]

The syntheses were conducted using a simple and low-cost modified precipitation method and the QDs were characterized by X-ray diffraction (XRD), high-resolution transmission electron microscopy (HRTEM), Fourier transform infrared (FTIR) spectrometry, thermogravimetric analysis (TGA) and elemental analysis. The effect of variable concentrations of MPS surfactant on the optical properties of the QDs was also investigated. An unexpected decrease in the band gap energy compared with the well-known effect of the reduction in the nanoparticle size, was obtained and gives a new insight into the relationship between the value of the band gap energy and the nature of the organic surfactant that promoted the reduction in nanoparticle size.

2. Experimental section

2.1 Materials and synthesis of ZnO QDs

Zinc acetate dihydrate (purity >98%), methanol, MPS (purity 98%) and potassium hydroxide were purchased from Sigma Aldrich and were used without further purification.

ZnO QDs were synthesized according to a slight modification of a previously reported precipitation method;[13] the detailed synthesis procedure is given in the ESI.† The samples obtained were labelled as ZnO–MPS *x*%, where *x* is the Si/Zn molar ratio used in the synthesis. The reference sample prepared without organic silane was simply labelled as ZnO.

2.2 Characterization methods

The XRD patterns were recorded for ground powders with an Empyrean diffractometer (PANalytical, The Netherlands) using Cu Kα1 (λ = 1.540598 Å) radiation, equipped with 2xGe(220) hybrid monochromator for Cu and a PIXcel3D detector. The analyses were performed using Bragg–Brentano geometry (θ–2θ) for angles between 10 and 80° 2θ degrees with a step size of 0.04° and an acquisition time for a step size of 3 s.

A small amount of each sample was mounted on a single-crystal silicon holder; this holder does not interfere with the diffraction in the analysis range for radiation emitted by a Cu anode. The sample was gently pressed onto the holder so that the area to be analysed was flat. Rietveld refinement was performed to identify the cell parameters and the mean crystallite size. The acceptance indexes considered for the refinement were: $R_{expected}$, $R_{profile}$, the weighted $R_{profile}$ and the goodness-of-fit. Table S1† gives the relevant crystallographic data for unmodified and MPS-modified ZnO nanoparticles.

The TEM images were obtained on finely powdered samples using a Tecnai G2 F30 S-TWIN high-resolution transmission electron microscope (FEI). The microscope was operated in the transmission mode at 300 kV with a point resolution of 2 Å and a line resolution of 1 Å. The finely ground ZnO powders were dispersed in pure ethanol and ultrasonicated for 15 min. The diluted sample was then put onto a carbon-coated copper grid and left to dry before analysis.

The FTIR spectra were recorded from 4000 to 650 cm^{-1} with a Perkin Elmer Spectrum 100 instrument using total reflectance on a ZnSe crystal (resolution 4 cm^{-1}).

The elemental analyses (C, H) were performed with a Fisons Instruments 1108 CHNS–O elemental analyser. The samples were dried *in vacuo* (50 °C, about 0.1 Torr) before analysis, until a constant weight was reached.

TGA was performed under a pure air atmosphere (gas flow-rate 25 mL min^{-1}) with a TA Instruments TGA Q5000 analyser. The samples were heated from room temperature to 700 °C at a heating rate of 5 °C min^{-1}.

The optical transmission and reflectance spectra were acquired at room temperature with a Perkin Elmer (Lambda 35) UV-visible-NIR spectrophotometer with a spectral range of 190–1100 nm. The spectrometer was operated in air at normal incidence. Samples were prepared by dispersing the nanoparticles in isopropanol by sonication and then depositing as thin films on a glass substrate by spin coating (2000 rev min^{-1}, 20 s). The optical band gap energy, E_g, was estimated from the fundamental absorption edge of the nanoparticle-based thin films, assuming a direct transition between the valence and conduction bands. The optical band gaps were determined from the dependency of the absorption coefficient, α, on the photon energy, $h\nu$, given by eqn (1):

$$(\alpha h\nu)^2 = A(h\nu - E_g), \quad (1)$$

where A is a parameter that depends on the probability of transition.[18–25] The absorption coefficient, α, was calculated by eqn (2):

$$\alpha = \frac{1}{d} \ln\left[\frac{(1-R)^2 + \sqrt{(1-R)^2 + 4R^2T^2}}{2T}\right] \quad (2)$$

where d is the film thickness, T is the transmittance and R is the reflectance of the investigated samples.[26–29]

The thickness of the deposed thin films was determined with a MII-4 interference microscope (Linnik) with an error ≤0.01 μm using the multiple-beam Fizeau fringe method.[30] The thickness of the thin films was about 258 nm.

The solid-state photoluminescence emission spectra were recorded at room temperature with a Perkin Elmer LS 45 luminescence spectrometer equipped with a pulsed Xe flash lamp. The photoluminescence spectra recorded in the range 400–800

nm were collected for an optimum excitation wavelength of 365 nm, where the emission responses for all samples were the most intense.

3. Results and discussion

3.1 Structure and morphology

The XRD patterns of all the samples (Fig. 1) show main diffraction peaks at 31.6, 34.4, 36.1, 47.4, 56.4, 62.6 and 67.9° 2θ, assignable to the (100), (002), (101), (102), (110), (103) and (112) planes, respectively, of the wurzite structure of ZnO.[31] Observation of the intensity and full width at half maximum (FWHM) of the main diffraction peaks on passing from unmodified ZnO to the maximum-loaded MPS-grafted ZnO QDs highlights the significant effect of MPS grafting on the structure of the ZnO nanoparticles. The XRD pattern of the unmodified ZnO shows well-resolved reflections, whereas a progressive broadening of the diffraction peaks can be observed for ZnO–MPS 2%, ZnO–MPS 5% and ZnO–MPS 10%. This may be a result of size reduction effects induced by the organic silane functionalization, together with a reduction in crystallinity.

The average crystallite size (L) of the synthesized ZnO QDs was estimated by applying the Debye–Scherrer equation, $B(2\theta) = (K\lambda)/(L\cos\theta)$, to the (100), (102) and (110) planes, where B is the FWHM, λ is the X-ray wavelength, θ is the diffraction angle and K is Scherrer's constant, the value of which is 0.89 for spherical particles.[32] A progressive decrease was seen in the estimated crystallite size from 7.57 nm for unmodified ZnO QDs to 5.24, 4.34 and 4.19 nm for ZnO QDs grafted with 2, 5 and 10% MPS, respectively.

HRTEM was used to assess the average particle size and morphology of the ZnO samples; Fig. 2 shows the micrographs along with the corresponding histograms. The selected area electron diffraction patterns of the ZnO QDs were also determined (Fig. S1†). All the diffraction rings were attributed to ZnO with a wurtzite structure in line with the XRD data. The HRTEM image of unmodified ZnO QDs (Fig. 2A) shows nearly spherical or ellipsoidal shapes. As indicated by the histogram in Fig. 2A′ (determined by measuring the diameter of more than 100 ZnO nanocrystals), the unmodified ZnO QDs were characterized by a particle size distribution centred at 10.67 ± 0.29 nm, which is slightly higher than the average size estimated from the XRD data. QDs with a similar morphology can be seen for all the organosilane-based ZnO samples. The HRTEM micrographs show that on changing from unmodified ZnO to organo-modified ZnO QDs the size significantly decreases (by about half) for QDs grafted with 2% MPS, whereas the increase in MPS concentration to 5 and 10% produces only small and insignificant decreases in nanoparticle size (Fig. 2B–D). Fig. 2B′ shows the histogram for ZnO–MPS 2% and the measured average diameter is centred at 4.02 ± 0.21 nm, close to the estimated value calculated from the XRD data. The histograms of ZnO–MPS 5% and ZnO–MPS 10% (Fig. 2C′ and 2D′) show very close values of the average diameter centred at 3.86 ± 0.09 nm and 3.85 ± 0.1 nm, respectively, and are also close to the estimated values calculated from the XRD data.

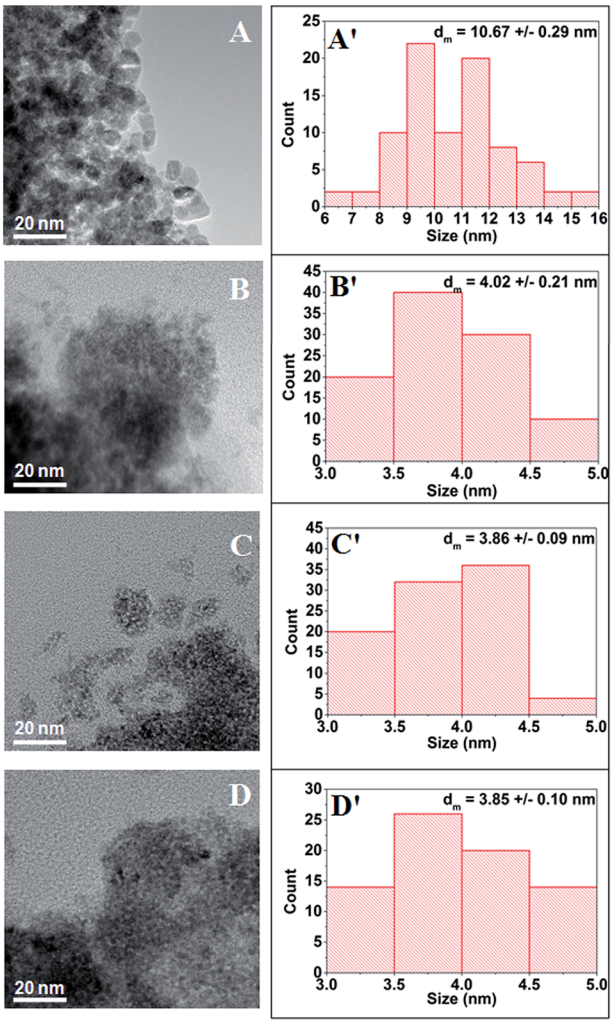

Fig. 2 HRTEM micrographs of (A) ZnO, (B) ZnO–MPS 2%, (C) ZnO–MPS 5% and (D) ZnO–MPS 10%; the histograms of the particle size of all samples are displayed in parts A′, B′, C′ and D′, respectively.

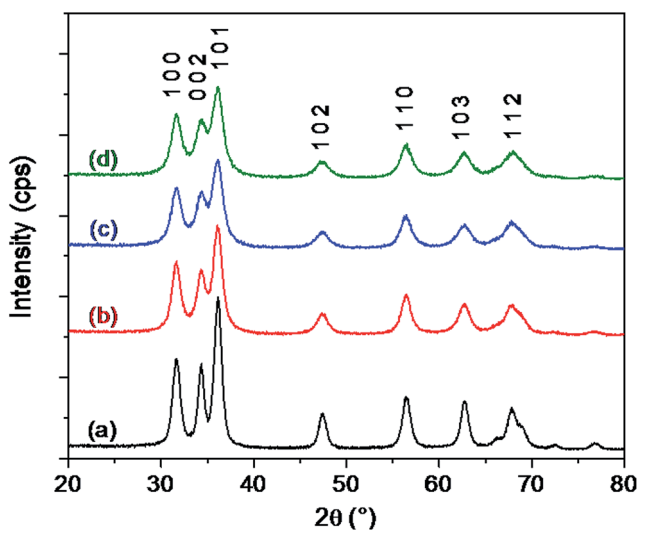

Fig. 1 XRD profiles of (a) ZnO, (b) ZnO–MPS 2%, (c) ZnO–MPS 5% and (d) ZnO–MPS 10%.

This shows that higher organosilane concentrations result in a smaller ZnO crystallite size and smaller grafted ZnO QDs. These results demonstrate that the amount of MPS introduced in the synthesis process influences not only the growth of the ZnO crystallites, but also the growth of the ZnO QDs. This effect of MPS can be explained by its direct participation in the condensation reaction with the $Zn(OH)_2$ and ZnO species, thus limiting the self-condensation of $Zn(OH)_2$ in the primary growth of ZnO crystallites and in their agglomeration (Scheme S1†).[13,14]

3.2 FTIR spectrometry

FTIR spectrometry was used to investigate the binding of the MPS molecules onto the surface of the ZnO QDs. Fig. 3 shows the IR spectra of both the unmodified ZnO and the organosilane-modified ZnO samples. A broad band in the range 3500–3000 cm^{-1} can be assigned to the stretching vibration of OH groups in the residual water physically adsorbed on the surface of the particles. Two strong bands at 1566 and 1416 cm^{-1} in ZnO, at 1562 and 1420 cm^{-1} in ZnO–MPS 2%, at 1567 and 1408 cm^{-1} in ZnO–MPS 5%, and at 1567 and 1409 cm^{-1} in ZnO–MPS 10% are assigned to the asymmetrical and symmetrical stretching modes of the carboxylate groups (COO^-) of residual acetate anions chemically attached to the ZnO surface during the synthesis process; these are difficult to remove completely, even with intense washing of the samples. The differences in frequency ($\Delta\nu = \nu_a - \nu_s = 150$ cm^{-1} in ZnO, 142 cm^{-1} in ZnO–MPS 2%, 159 cm^{-1} in ZnO–MPS 5% and 158 cm^{-1} in ZnO–MPS) most likely indicate a bridging coordination geometry.[33] However, a decrease in the intensity of the two bands is observed on moving from unmodified ZnO to ZnO–MPS 10% and is a result of the replacement of the residual carboxylate groups by MPS molecules. The broad peak at 892 cm^{-1} can be attributed to Zn–OH bonds formed by the chemical attachment of the hydroxy groups on the ZnO particles.

In the IR spectrum of free MPS (Fig. S2†), the bands at 1715, 1637 and 1161 cm^{-1} are assigned to the vibrations of the C=O, C=C and C–O bonds, respectively. In the spectra of MPS-treated ZnO QDs, the shift of the C=O stretch at 1702–1707 cm^{-1} and a minor shift in the C–O stretch at 1171 cm^{-1} indicate successful functionalization of the ZnO surface through chemical bonding. An increase in the intensity of these two specific bands on moving from simple ZnO to ZnO–MPS 10% can be observed. The presence of a very weak C=C stretch in the MPS-treated ZnO samples at 1632–1638 cm^{-1}, partially overlapped with the very strong asymmetric band of carboxylate, may suggest that no network polymerization takes place by cross-linking of the pendant methacrylate end-groups. Additional absorption bands at 1075 and 934 cm^{-1}, characteristic of Si–O–C bonds in free MPS, completely disappear in MPS-treated ZnO samples, indicating that condensation between the methyl groups from the trimethoxysilane moiety and the hydroxy groups on the ZnO surface has successfully occurred.[34]

The bands at 2838 and 2944 cm^{-1} belong to the aliphatic C–H bonds present in non-hydrolysed MPS, whereas in the MPS-grafted ZnO samples the bands observed in the range 2800–3000 cm^{-1} include the vibration stretching of the $-CH_2$ groups of the propyl chain bound to the silane moiety on the ZnO surface and also the $-CH_3$ groups from both the acetate anions and the methacrylate groups. The intense peak at 812 cm^{-1} in free MPS is characteristic of the symmetrical stretching of $Si-O-CH_3$, whereas in the MPS-based ZnO samples it disappears, suggesting the complete reaction between MPS and the hydrolysed ZnO particles. A new finely split and very strong band located at 878–884 cm^{-1}, which appears in the MPS-grafted ZnO samples, may indicate the formation of both Zn–O–Si bonds during the functionalization process and Si–O–Si bridges by self-condensation of the organosilanes used to modify the ZnO surface.[12] Fig. 4 is a sketch of a simplified structural model of the organosilane-treated ZnO QDs in which the condensed silane moieties

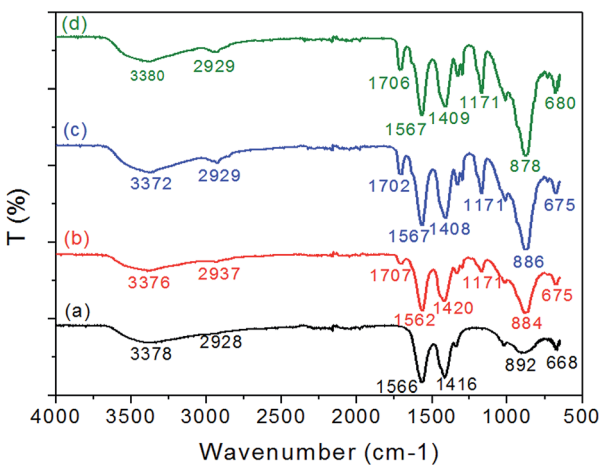

Fig. 3 FTIR spectra of (a) ZnO, (b) ZnO–MPS 2%, (c) ZnO–MPS 5% and (d) ZnO–MPS 10%.

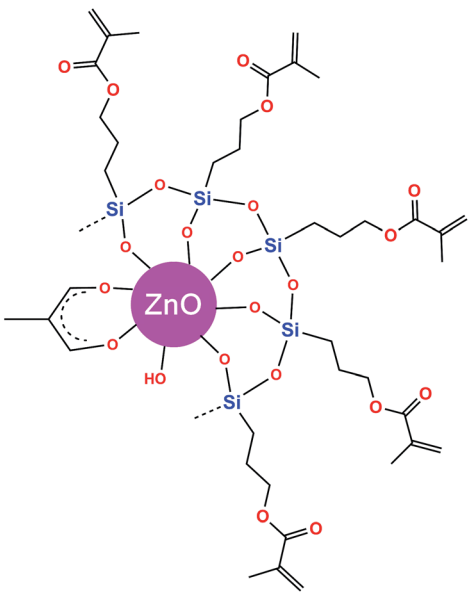

Fig. 4 Proposed structural model of the organosilane-treated ZnO nanoparticles.

give the shape of a cross-linked shell with the methacrylate groups oriented outwards.

3.3 Thermogravimetric analysis

The thermal behaviour of unmodified and organo-modified ZnO nanoparticles was investigated by TGA to assess their thermal stability and to identify the main weight losses occurring in the samples during the heating process. The TGA results, FTIR data and elemental analyses (C, H) were in agreement about the stoichiometric formulae of both the unmodified ZnO and MPS-treated ZnO samples (Table S1†).

The TGA profile of the unmodified ZnO sample (Fig. 5A, curve a) shows a first weight loss of 1.51% in the range 30–120 °C as a result of the evaporation of two water molecules physically adsorbed on the ZnO surface (theoretical weight loss 1.53%, in close agreement with the experimental value). The second weight loss of 0.73% in the range 120–220 °C can be attributed to the evolution of one water molecule, possibly from two hydroxy groups chemically attached to the ZnO surface (theoretical weight loss 0.76%). The third weight loss of 4.61% in the range 220–500 °C is due to the decomposition of the acetate anion, which may release acetone and carbon dioxide, as proposed by Hiltunen *et al.*[35] (theoretical weight loss 4.33%). The corresponding DTG curve (Fig. 5B, curve a) shows one peak at 53 °C assigned to the evaporation of physically adsorbed water molecules and one set of peaks at 296, 353 and 374 °C assigned to a more complex thermal decomposition of the acetate ions bound to the ZnO surface.

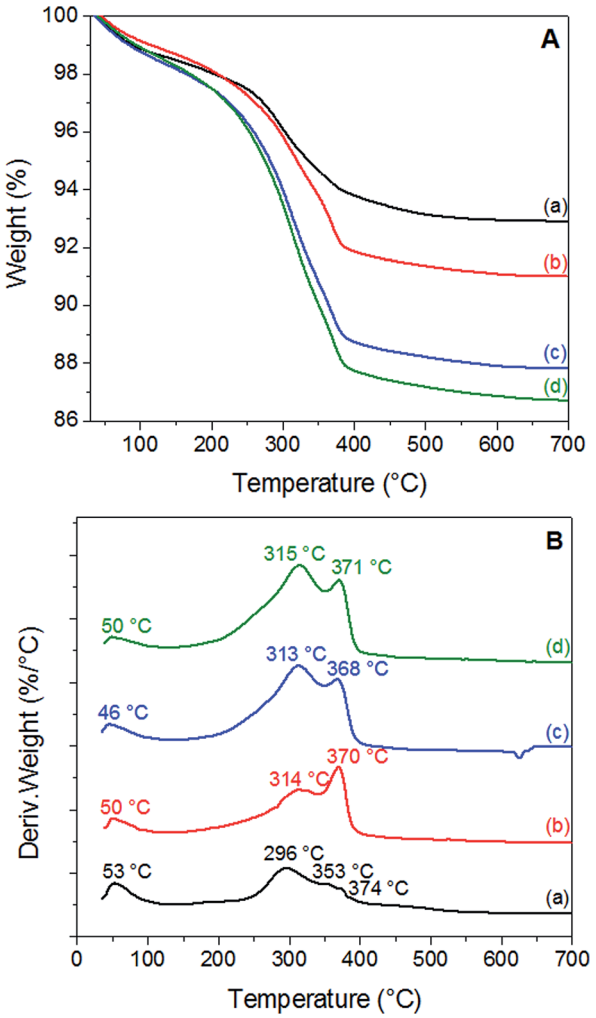

Fig. 5 (A) TGA and (B) DTG curves of (a) ZnO, (b) ZnO–MPS 2%, (c) ZnO–MPS 5% and (d) ZnO–MPS 10%.

The TGA profile of the ZnO–MPS 2% sample (Fig. 5A, curve b) shows a first weight loss of 1.18% in the range 30–120 °C as a result of the evaporation of two physically adsorbed water molecules onto the ZnO surface (theoretical weight loss 1.19%, in close agreement with the experimental value). A second weight loss of 1.17% in the range 120–220 °C can be attributed to the evolution of two water molecules from the condensation reaction, promoted by heating, of two zinc(II) hydroxide molecules present as trace amounts in the sample (theoretical weight loss 1.19%). A further cumulative weight loss of 6.57% in the range 220–500 °C can be assigned to the decomposition of both the acetate anion and the demethylated MPS that breaks into one propylmethacrylate ($C_7H_{11}O_3$) fragment and silicon dioxide (theoretical weight 6.68%). It is well known that the alkoxysilane group releases SiO_2 by thermal decomposition, as detected, for example, by Musat *et al.*,[36] who reported a thermal study of sol–gel precursors containing zinc acetate as a ZnO source and tetraethoxysilane as an SiO_2 source. The corresponding DTG curve (Fig. 5B, curve b) shows one peak at 50 °C assigned to the evaporation of physically adsorbed water molecules and one set of peaks at 314 and 370 °C assigned to the thermal decomposition of acetate ions and demethylated MPS bound to the ZnO surface.[14]

The TGA profile of the ZnO–MPS 5% sample (Fig. 5A, curve c) shows a first cumulative weight loss of 2.54% in the range 30–200 °C as a result of the removal of two physically adsorbed water molecules (1.02%) and three water molecules (1.52%) resulting from the condensation reaction, promoted by heating, of two zinc(II) hydroxide molecules present as trace amounts in the sample (theoretical weight loss 2.57%). A further cumulative weight loss of 9.67% in the range 220–500 °C is a result of the decomposition of both the acetate anion and demethylated MPS breaking into two propylmethacrylate fragments and silica (theoretical weight loss 9.85%). The corresponding DTG curve (Fig. 5B, curve c) shows one peak at 46 °C assigned to the evaporation of physically adsorbed water molecules and one set of peaks at 313 and 368 °C assigned to the thermal decomposition of acetate ions and demethylated MPS bound to the ZnO surface.[14]

The TGA profile of the ZnO–MPS 10% sample (Fig. 5A, curve d) shows a first cumulative weight loss of 3% in the range 30–220 °C as a result of the removal by evaporation of three physically adsorbed water molecules (1.07%) and five water molecules (1.93%) resulting from the condensation reaction, promoted by heating, of four zinc(II) hydroxide molecules present as trace amounts in the sample (theoretical weight loss 3.1%). A further cumulative weight loss of 10.27% in the range 220–500 °C is a result of the decomposition of both the acetate anion and demethylated MPS broken into three

propylmethacrylate fragments and silica (theoretical weight loss 10.86%). The corresponding DTG curve (Fig. 5B, curve d) shows one peak at 50 °C assigned to the evaporation of physically adsorbed water molecules and one set of peaks at 315 and 371 °C, assigned to the thermal decomposition of acetate ions and demethylated MPS bound to the ZnO surface.[14]

From an overall comparison of these TGA results, it can be observed that all the MPS-grafted ZnO QDs contained a very low amount of physically adsorbed water molecules in the narrow range 1–1.2% with respect to the unmodified ZnO sample. This suggests a remarkable hydrophobic character attained during successful functionalization. All the samples were stable up to 225 °C, as determined by the onset of decomposition around this temperature.

3.4 Optical properties

Fig. 6 shows the optical transmittance and reflectance spectra of the thin films based on unmodified ZnO and organosilane-modified ZnO samples in the UV-visible-NIR wavelength region (200–1100 nm). All these films, with a measured thickness of about 258 nm, show between 85 and 90% optical transmittance in the visible range. A slight increase in the optical transmittance of the MPS-modified ZnO nanoparticle-based thin films compared with the unmodified ZnO-based film is observed in the 400–800 nm range. This can be explained by the presence of the organosilane surfactant, which contributes to the transparency of the resultant hybrid thin films. The increase in transmittance in the visible domain is also associated with the decreased size of the nanoparticles and their decreased agglomeration.

Fig. 7 shows a decrease in the band gap energy of the MPS-modified ZnO nanoparticles compared with the unmodified ZnO nanoparticles. A continuous decrease was observed with increasing MPS concentration, from 3.494 eV for the unmodified ZnO nanoparticles to 3.377 eV for the 10% MPS-modified ZnO nanoparticles. The value of 3.494 eV is consistently higher than the 3.37 eV obtained for bulk ZnO samples. These high values have also been reported for ZnO nanostructures.[37]

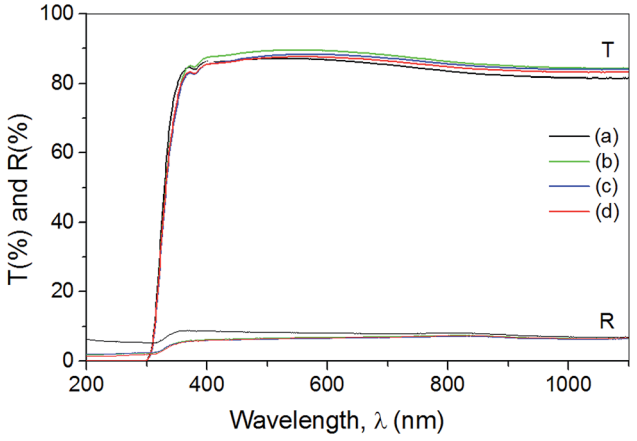

Fig. 6 Optical transmittance and reflectance spectra of (a) ZnO, (b) ZnO–MPS 2%, (c) ZnO–MPS 5% and (d) ZnO–MPS 10%.

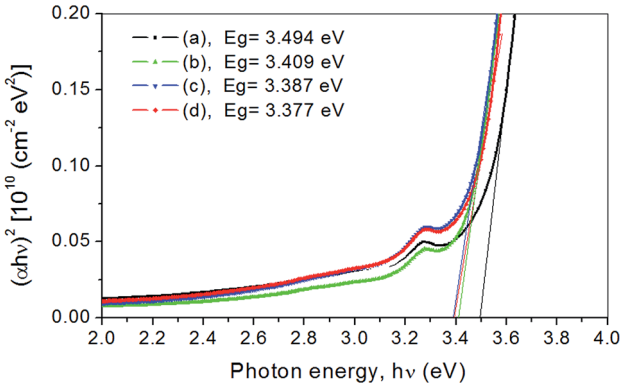

Fig. 7 Plots of $(\alpha h\nu)^2$ *versus* photon energy ($h\nu$) of (a) ZnO, (b) ZnO–MPS 2%, (c) ZnO–MPS 5% and (d) ZnO–MPS 10%.

The largest variation in the band gap of 0.085 eV (from 3.494 to 3.409 eV) was observed when ZnO QDs were grafted with 2% MPS, which showed the largest decrease in size (by half) relative to the unmodified ZnO. Increasing the MPS concentration from 2 to 5% and from 5 to 10% caused smaller variations of 0.02 and 0.01 eV, respectively, in agreement with the very small change in the size of the nanoparticles (Fig. 2A–D). This nearly exponential decay may be explained by the variation in the composition and morphology of the films as a function of the grafting concentration.[38]

The emission properties of the unmodified and organosilane-modified ZnO materials were compared. Fig. 8 shows the photoluminescence spectra of all the samples obtained by irradiation at 365 nm. The unmodified ZnO sample shows a wide emission band centred at about 578 nm, which is associated with the electronic transitions of surface defects, such as zinc and oxygen vacancies, interstitial zinc and/or oxygen atoms.[39,40] The ZnO–MPS 2% sample displays a much more intense emission band with respect to the unmodified sample, with a maximum centred at about 556 nm. As the

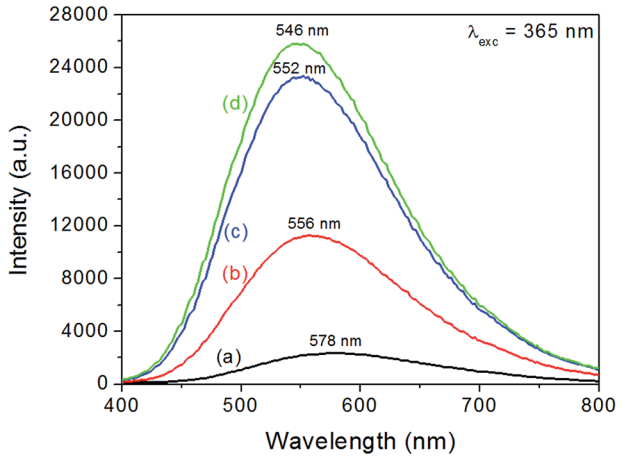

Fig. 8 Solid-state photoluminescence spectra of (a) ZnO, (b) ZnO–MPS 2%, (c) ZnO–MPS 5% and (d) ZnO–MPS 10% obtained with an excitation wavelength of 365 nm.

organosilane loading increases, a blue shift and subsequent increase in the emission intensity is observed for the highest loaded ZnO–MPS 10% sample, showing the most intense emission band with a maximum centred at 546 nm. The most important variation in relation to the unmodified ZnO sample occurs for a 2% addition of MPS. The blue shift in the emission bands can be related to a decrease in the particle size of the MPS-modified ZnO samples, as previously reported for organosilane-modified ZnO samples.[41,42]

Functionalization of the ZnO surface may also be an additional factor in triggering a further increase and/or modification of the surface defects.[43,44] A certain type of electronic relaxation causes such a broad emission band in which the photogenerated holes are trapped inside the surface O^{2-}/O^{-} states. Through tunnelling processes and subsequent recombination with the oxygen vacancies, these trapped holes are able to return to the bulk phase. Consequently, this recombination promotes the emission effect in the visible domain, becoming more intense for the smaller ZnO nanoparticles.[45] Fig. 9 shows digital photographs obtained under UV irradiation at 365 nm for both unmodified ZnO and the organosilane-modified ZnO powders. As expected, based on the photoluminescence spectra, the unmodified ZnO sample shows the weakest emission, whereas the ZnO–MPS 5% and ZnO–MPS 10% samples have the strongest emissions.

The surface modification of ZnO nanoparticles through functionalization with the MPS organosilane species is therefore a useful tool for tuning the photoluminescence efficiency and emission wavelength. Surface functionalization with organosilane during the growth process can significantly reduce the aggregation of the particles, promoting an increase in the number of effective surface luminescence centres.

From the point of view of the photoluminescence mechanism, it is assumed that electron transitions from the conduction band to a deeply trapped defect state trigger the visible emission. It has been previously reported that, as the size of the ZnO nanoparticles becomes smaller during functionalization with organic surfactants, the band gap energy increases as a result of quantum size effects.[10] To the best of our knowledge, there has been no other published report of the experimental determination of the band gap energy for organo-modified ZnO nanoparticles; this has previously only been mentioned as a generally accepted trend. Our results for the determination of the band gap values for unmodified ZnO and MPS-treated ZnO nanoparticles (Fig. 7) showed the reverse: the size reduction in the MPS-grafted ZnO QDs results in decreased band gap energies (Fig. 10). For ZnO nanoparticles grafted with the MPS surfactant, which has oxygen atoms with free electrons in lone pairs in its structure, two opposite effects take place at the level of the ZnO electronic bands with increasing surfactant concentration: (1) shrinking of both the valence and conduction bands as a result of the decrease in size of the ZnO nanoparticles and (2) enlargement of the bands as determined by electron injection from the oxygen atoms (with lone pairs) of the MPS bound to the surface of the ZnO nanoparticles.

The dark areas in the valence and conduction bands in Fig. 10 represent fine splitting of the energy levels populated by electrons injected from the capping organosilanes. This splitting is a result of the quantum confinement effect, which is specific to QDs.[46]

Taking into account the decrease in the band gap energies with the concentration of MPS, it can be shown that the enlargement of the bands by electron injection compensates, and even overcomes, the reduction effect of the size of the ZnO nanoparticles. *Silane-coupling* agents are known to be external or *electron donors*. Previously published papers have mentioned that the use of silane-coupling reagents for the strong chemical fixation of dyes on, for example, TiO_2 nanoparticles, may enhance the injection of electrons into nanocrystalline semiconductor particles, resulting in the transfer of intramolecular energy from highly absorbing chromophore groups and, consequently, improving the photosensitized efficiency.[47–50] The raising of the HOMO level by incorporating donor ligands is one of the strategies successfully applied in designing sensitizers which absorb over the whole visible spectrum for applications in dye-sensitized solar cells and sensitized photocatalysts for environmental purification.[47]

With the increase in surfactant concentration as a result of the reduction in nanoparticle size, there is a limit to the number

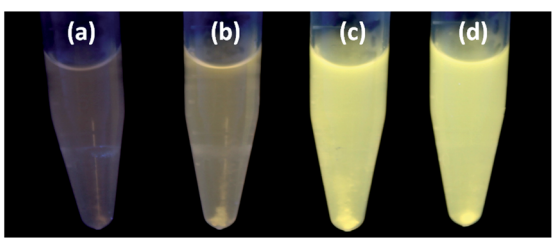

Fig. 9 Digital photographs of (a) ZnO, (b) ZnO–MPS 2%, (c) ZnO–MPS 5% and (d) ZnO–MPS 10% powders dispersed in isopropanol under UV irradiation at 365 nm.

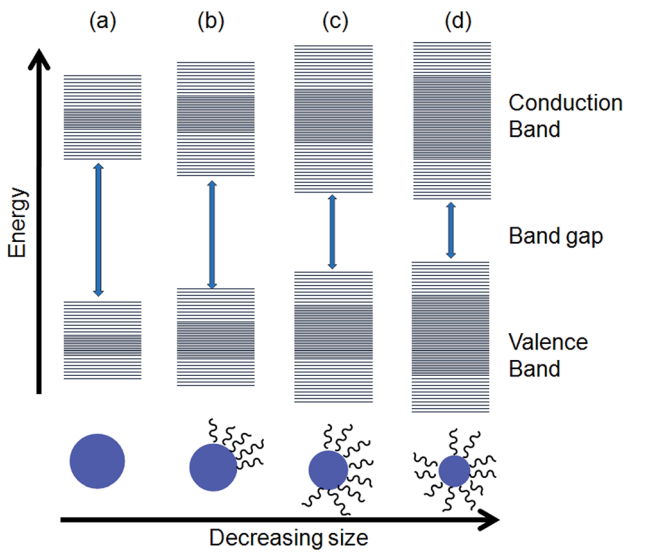

Fig. 10 Schematic representation of the band structures of (a) ZnO, (b) ZnO–MPS 2%, (c) ZnO–MPS 5% and (d) ZnO–MPS 10%.

of MPS molecules attached on their surfaces. This overlap of effects explains the fact that the reduction in the band gap is not proportional to the concentration of surfactant. This reduction becomes increasingly smaller at high concentrations – it is significant at 2% MPS grafting and increasingly lower at higher MPS concentrations of 5% and 10%. This unexpected result gives a new insight into the relationship between the reduction in nanoparticle size promoted by the organic surfactant and the value of the band gap energy. The close values of the band gaps for the samples grafted with 5 and 10% organosilane correlated with the photoluminescence intensities shows that there is a limit to the injection of electrons. We observed experimentally that an organosilane loading >10% cannot be attained and therefore the saturation limit of organosilane loading remains fixed at this percentage.

4. Conclusion

Hybrid organosilane-grafted ZnO QDs have been successfully fabricated on a surface attachment of MPS surfactant through a modified precipitation method. These QDs demonstrate remarkable hydrophobicity, high transmittance values and variable emission intensities in the visible domain under UV irradiation. A decrease in the band gap energies was detected, from 3.494 eV for unmodified ZnO to 3.377 eV for ZnO–MPS 10%. The 5 and 10% MPS-grafted ZnO nanoparticles showed the best emission properties and are promising candidates as active layers in hybrid light-emitting devices for optoelectronic applications.

Acknowledgements

The work of Aurel Tăbăcaru was funded by the Sectoral Operational Programme Human Resources Development 2007–2013 of the Ministry of European Funds through Financial Agreement POSDRU/159/1.5/S/132397. Professor Nicolae Tigau, Professor Rodica Dinica, Dr Mariana Busila and PhD student Viorica Ghisman from the "Dunărea de Jos" University of Galati (Romania), as well as PhD student Nertil Xhaferaj and Professor Claudio Pettinari from the University of Camerino (Italy), are gratefully acknowledged for helpful experimental assistance and discussions.

Notes and references

1 U. Ozgur, Y. I. Alivov, C. Liu, A. Teke, M. A. Reshchikov, S. Dogan, V. Avrutin, S.-J. Cho and H. Morkoc, *J. Appl. Phys.*, 2005, **98**, 041301.
2 J. Mawyin, Y. Shupyk, M. Wang, G. Poize, P. Atienzar, T. Ishwara, J. R. Durrant, J. Nelson, D. Kanehira, N. Yoshimoto, C. Martini, E. Shilova, P. Secondo, H. Brisset, F. Fages and J. Ackermann, *J. Phys. Chem. C*, 2011, **115**, 10881.
3 E. Fortunato, P. Barquinha and R. Martins, *Adv. Mater.*, 2012, **24**, 2945.
4 M. Karimi, J. Saydi, M. Mahmoodi, J. Seidi, M. Ezzati, S. Shamsi Anari and B. Ghasemian, *J. Phys. Chem. Solid*, 2013, **74**, 1392.
5 Y. Martynova, B.-H. Liu, M. E. McBriarty, I. M. N. Groot, M. J. Bedzyk, S. Shaikhutdinov and H.-J. Freund, *J. Catal.*, 2013, **301**, 227.
6 X. Tang, E. S. G. Choo, L. Li, J. Ding and J. Xue, *Langmuir*, 2009, **25**, 5271.
7 D. M. Yebra, S. Kiil, C. E. Weinell and K. Dam-Johansen, *Prog. Org. Coat.*, 2006, **56**, 327.
8 M. Ibanescu (Busila), V. Musat, T. Textor, V. Badilita and B. Mahltig, *J. Alloys Comp.*, 2014, **610**, 244.
9 M. Monge, M. L. Kahn, A. Maisonnat and B. Chaudret, *Angew. Chem., Int. Ed.*, 2003, **42**, 5321.
10 N. S. Pesika, Z. Hu, K. J. Stebe and P. C. Searson, *J. Phys. Chem. B*, 2002, **106**, 6985.
11 S. Tachikawa, A. Noguchi, T. Tsuge, M. Hara, O. Odawara and H. Wada, *Materials*, 2011, **4**, 1132.
12 A. Aboulaich, C.-M. Tilmaciu, C. Merlin, C. Mercier, H. Guilloteau, G. Medjahdi and R. Schneider, *Nanotechnology*, 2012, **23**, 335101.
13 M. Kotecha, W. Veeman, B. Rohe and M. Tausch, *Micropor. Mesopor. Mater.*, 2006, **95**, 66.
14 C. Bressy, V. G. Ngo, F. Ziarelli and A. Margaillan, *Langmuir*, 2012, **28**, 3290.
15 H.-C. Huang and T.-E. Hsieh, *Ceram. Int.*, 2010, **36**, 1245.
16 Z. Guo, S. Wei, B. Shedd, R. Scaffaro, T. Pereira and H. T. Hann, *J. Mater. Chem.*, 2007, **17**, 806.
17 R. Ciriminna, A. Fidalgo, V. Pandarus, F. Beland, L. M. Ilharco and M. Pagliaro, *Chem. Rev.*, 2013, **113**, 6592.
18 O. S. Heavens, *Optical properties of thin solid films*, Butterworths, London, 1955.
19 E. Shanti, E. Dutta, A. Banerjee and K. L. Chopra, *J. Appl. Phys.*, 1981, **51**, 6243.
20 D. Bhattacharyya, S. Chaudhuri and A. K. Pal, *Vacuum*, 1992, **43**, 313.
21 V. Srikant and D. R. Clarke, *J. Appl. Phys.*, 1997, **81**, 6357.
22 S. T. Tan, B. J. Chen, X. W. Sun, W. J. Fan, H. S. Kwok, X. H. Zhang and S. J. Chua, *J. Appl. Phys.*, 2005, **98**, 013505.
23 T. Prasada Rao and M. C. Santhoshkumar, *Appl. Surf. Sci.*, 2009, **255**, 4579.
24 N. Ghraïri, F. Aousgi, M. Zribi and M. Kanzari, *Calchogenide Letters*, 2010, **7**, 217.
25 M. Mazhdi and P. Hossein Khani, *Int. J. Nano Dimens.*, 2012, **2**, 233.
26 D. K. Schroeder, *Semiconductor materials and device characterisation*, Wiley, 1990.
27 J. F. Muth, J. H. Lee, I. K. Shmagin, R. M. Kolbas, H. C. Casey, B. P. Keller, U. K. Mishra and S. P. DenBaars, *Appl. Phys. Lett.*, 1997, **71**, 2572.
28 C. H. Huang, G. Zhang, Z. Q. Chen, X. J. Huang and H. Y. Shen, *Opt. Laser Technol.*, 2002, **34**, 209.
29 V. Pena-Mendez, M. T. S. Nair and P. K. Nair, *Semicond. Sci. Technol.*, 2006, **21**, 450.
30 K. L. Chopra, *Thin Film Phenomena*, McGraw-Hill, New York, 1969.

31 R. Brayner, S. A. Dahoumane, C. Yepremian, C. Djediat, M. Meyer, A. Coute and F. Fievet, *Langmuir*, 2010, **26**, 6522.
32 A. L. Patterson, *Phys. Rev.*, 1939, **56**, 972.
33 K. Nakamoto, *Infrared and Raman spectra of inorganic and coordination compounds, Part B*, 6th edn, Wiley, 2009.
34 E. Tang, H. Liu, L. M. Sun, E. Zheng and G. X. Cheng, *Eur. Polym. J.*, 2007, **43**, 4210.
35 L. Hiltunen, M. Leskelä, M. Mäkelä and L. Niinistö, *Acta Chem. Scand., Ser. A*, 1987, **41**, 548.
36 V. Musat, P. Budrugeac and C. Gheorghies, *J. Therm. Anal. Cal.*, 2008, **94**, 373.
37 A. H. Moharram, S. A. Mansour, M. A. Hussein and M. Rashad, *J. Nanomater.*, 2014, 716210.
38 F. K. Shan and Y. S. Yu, *J. Eur. Ceram. Soc.*, 2004, **24**, 1869.
39 K. Vanheusden, W. L. Warren, C. H. Seager, D. R. Tallant, J. A. Vogit and B. E. Gnade, *J. Appl. Phys.*, 1996, **79**, 7983.
40 M. K. Patra, M. Manoth, V. K. Singh, G. Siddaramana Gowd, V. S. Choudhry, S. R. Vadera and N. Kumar, *J. Lumin.*, 2009, **129**, 320.
41 H.-Q. Shi, W.-N. Li, L.-W. Sun, Y. Liu, H.-M. Xiao and S.-Y. Fu, *Chem. Commun.*, 2011, **47**, 11921.
42 D. Costenaro, F. Carniato, G. Gatti, L. Marchese and C. Bisio, *New J. Chem.*, 2013, **37**, 2103.
43 L. Guo, S. Yang, C. Yang, P. Yu, J. Wang, W. Ge and G. K. L. Wong, *Appl. Phys. Lett.*, 2000, **76**, 2901.
44 K. Borgohain and S. Mahamuni, *Semicond. Sci. Technol.*, 1998, **13**, 1154.
45 A. van Dijken, E. A. Meulenkamp, D. Vanmaekelbergh and A. Meijerink, *J. Lumin.*, 2000, **87–89**, 454.
46 S. M. Reimann and M. Manninen, *Rev. Mod. Phys.*, 2002, **74**, 1283.
47 D. Pei and J. Luan, *Int. J. Photoenergy*, 2012, 262831.
48 F. Liu and G. J. Meyer, *Inorg. Chem.*, 2005, **44**, 9305.
49 Y. S. Chen, C. Li, C. H. Zheng, W. B. Wang, X. S. Wang and B. W. Zhang, *J. Mater. Chem.*, 2005, **15**, 1654.
50 T. Peng, K. Dai, H. Yi, D. Ke, P. Cai and L. Zan, *Chem. Phys. Lett.*, 2008, **460**, 216.